# BONAPARTE robot: improving the reproducibility and identifying critical parameters of the synthesis of gold nanoparticles

Asen Dankov, Laurin Hensen, Mert Aydin, Namhyun Choi, Helene Giesler, Dennis Toker, Sebastian Schlücker*, Roland Grzeschik*

* corresponding authors

Sebastian Schlücker, University of Duisburg-Essen, Essen, Germany, sebastian.schluecker@uni-due.de

Roland Grzeschik, University of Duisburg-Essen, Essen, Germany, roland.grzeschik@uni-due.de

## Abstract

In order to exploit the unique optical properties of gold nanoparticles, precise size and shape control is required. We have designed and constructed the highly customizable BONAPARTE (BOttom-up NAnoPARTiclE synthesis robot, which consists of components that are easy to obtain and cost-effective. Using the robot, critical reaction parameters such as pipetting speed, position and delays were examined. We found that the effect of both the pipetting speed and position have an influence on the final gold cluster size. The effect of the cluster size on the length of gold nanorods was investigated in a two-step seed-growth synthesis. Additionally, we showed time-critical steps in the synthesis of gold nanostars, can be performed with superior accuracy by the robot. Overall, the robot displayed improved reproducibility when compared to nanoparticle synthesis performed manually by persons of different experience.

## Introduction

Gold nanoparticles (AuNP) have attracted the interest of the scientific community due to a combination of physical and chemical properties that makes them unique. They biocompatible[1, 2] and interact strongly and size-dependently with light (plasmonics)[3], which facilitated uses in medicine[4], spectroscopy[5] and others.[4] Another equally important aspect is that their properties can be enhanced and tailored with appropriate functionalization for a specific purpose. [6] Spherical gold nanoparticles exhibit LSPR (localized surface plasmon resonance) band in the 500-550 nm range, however, the LSPR peak wavelength can be shifted to higher wavelengths by using anisotropic nanoparticles. For example, gold nanorods have an aspect-ratio dependent plasmonic peak that can be tuned to coincide with the near-infrared window of water. [7] Together with excellent biocompatibility and stability, it can be leveraged in photothermal therapy applications [8], bio-imaging [9] and diagnostics [10]. However, the particle properties are also very sensitive towards the actual particle distribution in terms of size and shape. This means that in order to achieve the desired performance for a specific application a narrow size and shape distribution is required. [11, 12] Monodispersity, yield, and shape control have been some of the issues that have plagued nanoparticle synthesis and AuNP in particular. [13–15] This is one of the reasons researchers have turned towards automation as a mean towards the improvement of the accuracy and reproducibility of the synthesis. [16, 17]

Arguably, the most straightforward way to automate a synthesis is to use a fluidic type of reactor, since it requires the least number of components. In principle, the bare minimum configuration of such a reactor can consist of a syringe pump, appropriate tubing, and mixing elements.[18] The relative simplicity comes, however, at a cost in terms of certain limitations including: 1) fouling issues in microfluidic reactors, 2) broad residence time and 3) low parallelism . [19] Another approach to the synthesis is the repurposing and utilization of liquid handlers (LiHa's), which are have been previously used, e.g. for the preparation of quantum dots, such as CdSe nanocrystals [20, 21] and lipid nanoparticles [22] in the field of biology. These are usually cartesian robots capable of high throughput pipetting with limited sample conditioning and characterization features. Due to components of the reactors requiring a high level of engineering and reliability, the cost of these devices is in the mid-to-high 5-digit range. This raises the question in terms of cost-effectiveness when considering that additional work is required to further adapt the system to the needed functionality requirements. Recently, 3D printing has become increasingly popular for rapid prototyping of complex parts.

Components can be designed and manufactured in-house on an inexpensive 3D printer, greatly speeding up testing and integration. Therefore, 3D printing can provide more headroom in terms of cost for device construction.

A custom-built synthesis robot, that consists partially of 3D-printed parts was reported by the Cronin group. [23] Additionally, the robot uses genetic learning algorithms to explore the chemical space of different gold nanoparticle syntheses. The combination of machine and deep learning models combined with the throughput and reproducibility of the robotic systems has been also shown by Zhao et al.[24] The robotic platform presented by them can search in the internet for literature, extracts synthesis data, processes the data into an execution protocol and performs the syntheses. A comprehensive examination of the synthesis with a focus on the critical parameters in the chemical space (e.g. concentrations/volumes of educts) was made. They found pairwise relationships between educt amounts in the synthesis of gold nanorods, which significantly affected the resulting particles. Both systems, however, utilize expensive components with the one presented by Zhao et al. incorporating both a cartesian robot and a robotic arm.

These studies almost exclusively investigate the chemical space as a way to improve the synthesis products. In contrast the systematic exploration of the process parameter space (e.g. temperatures, stirring conditions) by robotic systems has not been performed [25] although of equal importance. It is also rarely quantified – often reported expressions such as “gently” or “vigorously” stirring/shaking, “rapidly” added can be executed differently by different persons. For example, parameters such as pipetting speed cannot be fully quantified since manual pipettes lack feedback and setting capabilities. Even when using electronic pipettes, this parameter is rarely accessible. When a reaction takes place in under a second, as in the case of gold cluster synthesis with sodium borohydride as a reducing agent, the importance of precise execution increases. Among others, these factors have played a major role in the so-called “Reproducibility crisis” which results in: 1) 70% of scientists are not able to reproduce other’s work and 2) strikingly more than 50% cannot reproduce their own work consistently. [26] We observed these issues by splitting researchers in our group into two different categories of proficiency. It was found that the synthesis reproducibility of less skilled members (often bachelor's or master's students) was significantly poorer compared to the gold nanorod synthesis results performed by more proficient members (often doctoral students or postdoctoral researchers). Thus, arises the need for reproducibility improvements, quantification, and understanding of the significance of process parameters, which could be achieved by employing a synthesis robot. To address these issues, we developed the BONAPARTE synthesis robot to identify and quantify synthesis-related parameters, whose role was previously underestimated or unknown and to improve the reproducibility of the synthesis. As a result, this study reduced the amount of work required for synthesis and improved the quality of the nanoparticles produced.

## Results and discussion

An overview of the setup of the synthesis robot is shown in Figure 1a. It consists of a basic cartesian system and operates two home-built automated pipettes. The work area contains spare pipette tips (Eppendorf Combitips®), a Peltier cooler, a 12-position synthesis module, and an educts module (Figure 1a). A full feature list can be found in Table 1. Arguably, the most critical component is the pipette for dosing of chemicals. Without precise chemical dosing, no chemical reaction can be accurately reproduced. Small errors in the pipetting of chemicals in large excess may not exert significant effects. However, most steps are critical down to a sub-microliter (corresponding to a nanomole at the concentrations used). Therefore, we developed a custom automated pipette with tip replacement function. It consists of two clamps (Figure 1B), a bottom clamp which grips the main body of the pipette tip and a top clamp which grips the plunger. The robot can perform a synthesis once stock solutions are placed into its inventory. This is a step that requires human input, since the robot does not have a powder dispensing system for the preparation of stock solutions from a solid phase.

Table 1 Features of the BONAPARTE robot.

| Features | BONAPARTE |
|---|---|
| Reactor units | 12 |
| Stirring speed | 500-1500 |
| Heating | RT - 100°C |
| Cooling | Peltier (-18°C) |
| Pipetting | Dual pipettes with automatic pipette tip replacement |
| Pipetting volumes | 0.1 mL - 50 mL |
| Pipetting speeds | up to 40 mL/s |

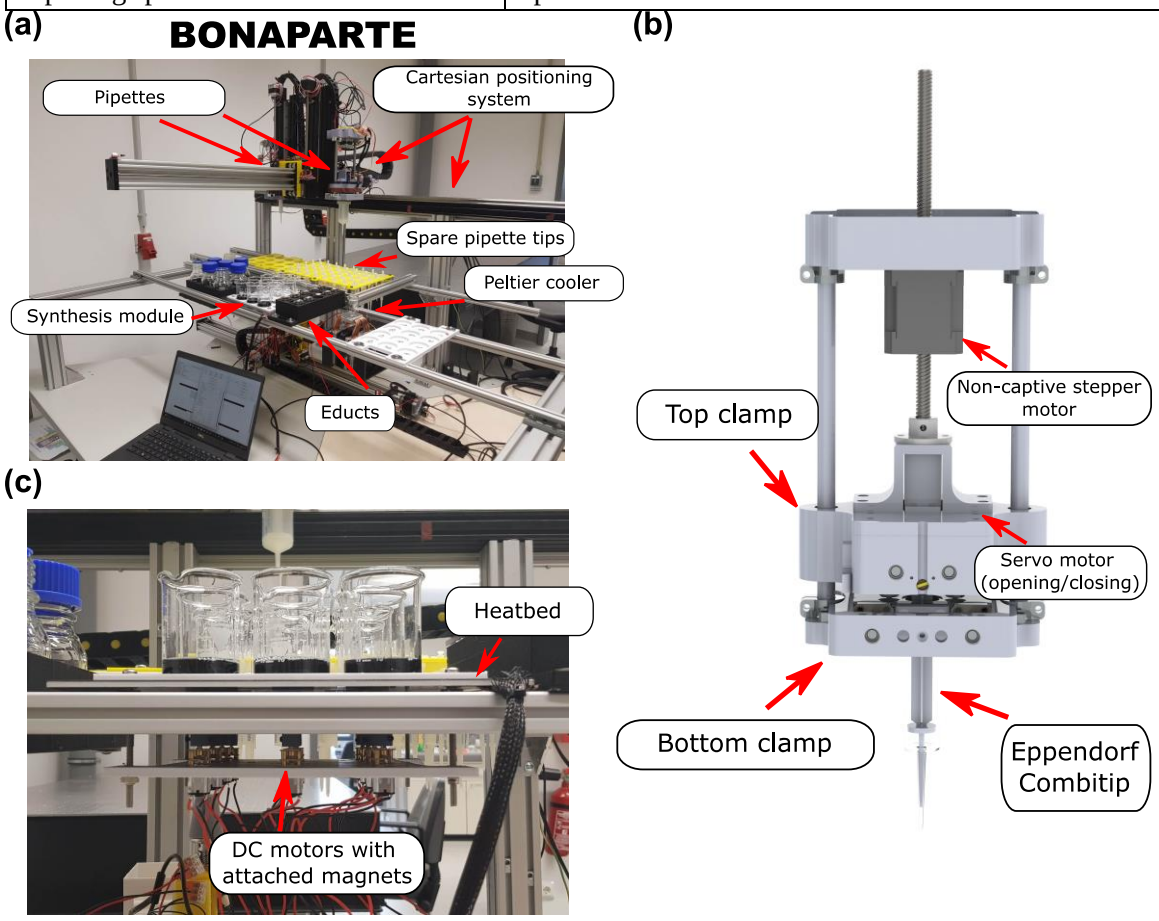


Figure 1 a) overview of the cartesian robot comprising a dual pipette system, spare pipettes, a cooler module, educts and a synthesis module with 12 synthesis units; b) automated pipette setup; c) close-up view of the synthesis module. DC motors with attached magnets are used for the stirring and a heat bed is utilized to regulate the temperature of a sample.

The flexibility and the design of the robot specifically allows the testing of less explored process parameters such as pipetting speed and position, but also custom timing of pipetting operations. The addition speed of reagents has been studied by Jana et al. [27] and Huang et al. [28] in a semiquantitative fashion, while Muralidharan et al. [25] and Besenhard et al. [29] used syringe pumps for additions speeds below 1.2 mL/s, which is comparable to slow pipetting by hand. The automated pipettes of BONAPARTE allow pipetting speeds of up to 40 mL/s to be executed, a range which is not accessible by hand or by normal syringe pump systems. The automated pipettes were also compared to manual and electronic pipettes used in our laboratory in term of precision and accuracy.

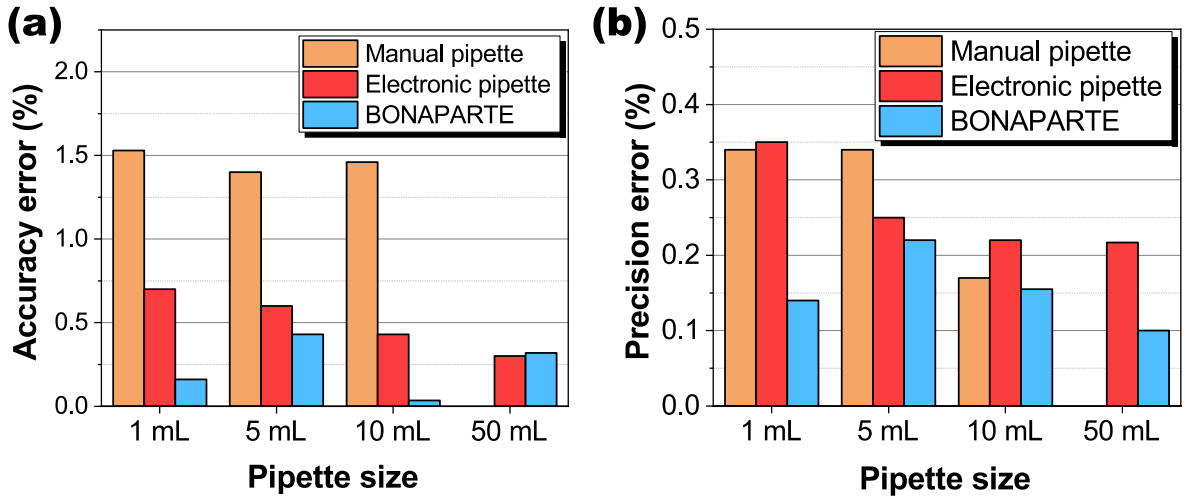


Figure 2 Pipette accuracy and precision compared the common manual and electronic laboratory pipettes. A 50 mL manual pipette was not available for testing.

To evaluate the performance of the robot, we chose synthesis protocols that are difficult for humans to execute and lack specific numerical values for process parameters. The first step is a synthesis of gold clusters, which is a reaction that happens in under a second and thus requires highly precise execution. The second is a gold nanorods synthesis, which uses the previously synthesized clusters as seeds. The third is a synthesis of nanostars via the hydroquinone route, which contains a critical step where two educts have to be pipetted in quick succession, but also doesn't provide sufficient detail in terms of how quick the addition of the second educt has to be performed. We compared robotic and manual synthesis. The process of manual synthesis was carried out in batches, with each batch being separated into three groups depending on the level of laboratory expertise: low, average, and high. A table on the experience classification can be found in the supporting information (Table S1).

**Synthesis of gold clusters**

Small gold clusters are often employed in the seed-mediated synthesis of anisotropic particles, such as gold nanorods. Due to the possibility of error propagation from the clusters (first step) to the rods (second step), attention was paid to the execution of the first step. First, the synthesis results of the robot were compared with the manual synthesis (see Figure 3a-d). In the case of gold clusters, the UV-Vis extinction spectrum is relatively featureless, with only a shoulder at 360 nm being distinguishable. Therefore, we compared the spectra of multiple syntheses performed by hand and by the robot in terms of the average standard deviation. Figure 3a-d shows the results based on the UV-Vis extinction spectra. The corresponding synthesis was repeated between 6 to 15 times. In order for the comparison to be fair, the robot's parameters for the synthesis were programmed as close as possible to how the manual synthesis should be performed. Initially, we approximated a pipetting speed of 4 mL/s (most rapid injection via manual pipette) and an offset of 5 mm to avoid pipetting directly in the middle of the vortex. Since the stock solutions are prepared manually in between batches, it is important to be careful when weighing compounds, as any error at this stage could potentially impact the final results. These errors could also propagate to the results of the robot. Therefore, the robot's syntheses are evaluated both batch-to-batch and intrabatch. The improvement based on the average standard deviation of the UV-Vis extinction spectra is shown in Figure 3e. The performance of all groups is better than the "low" group, whereas the robot and the "high" group show similar performance. The intrabatch performance of BONAPARTE was almost twice as good as the "high" group's performance and the robot batch-to-batch performance. This indicates a high probability of errors during the preparation of the stock solution influencing the resulting nanoparticles and, thereby, their UV-Vis extinction spectra. In order to realize the robot's intrabatch improvement of above 4x consistently, the factor of human error during the preparation of stock solutions has to be eliminated. This can be realized by an integration of a powder dispensing system and scale for the weighing of chemicals in powder form. Some stock solutions such as chloroauric acid could be stored for longer periods if refrigerated, while others such

as $NaBH_4$ are always prepared shortly before the synthesis. Integrating a refrigerated chamber into the robot could provide a solution for long-term storage not only of stock solutions, but possibly also products that need refrigeration, such as bioconjugated nanoparticles.

However, the intrabatch improvements also point towards a more reproducible pipetting by the robot, not only in terms of pipetting accuracy but possibly due to the precise pipetting with the same preset speed and position by the robot.

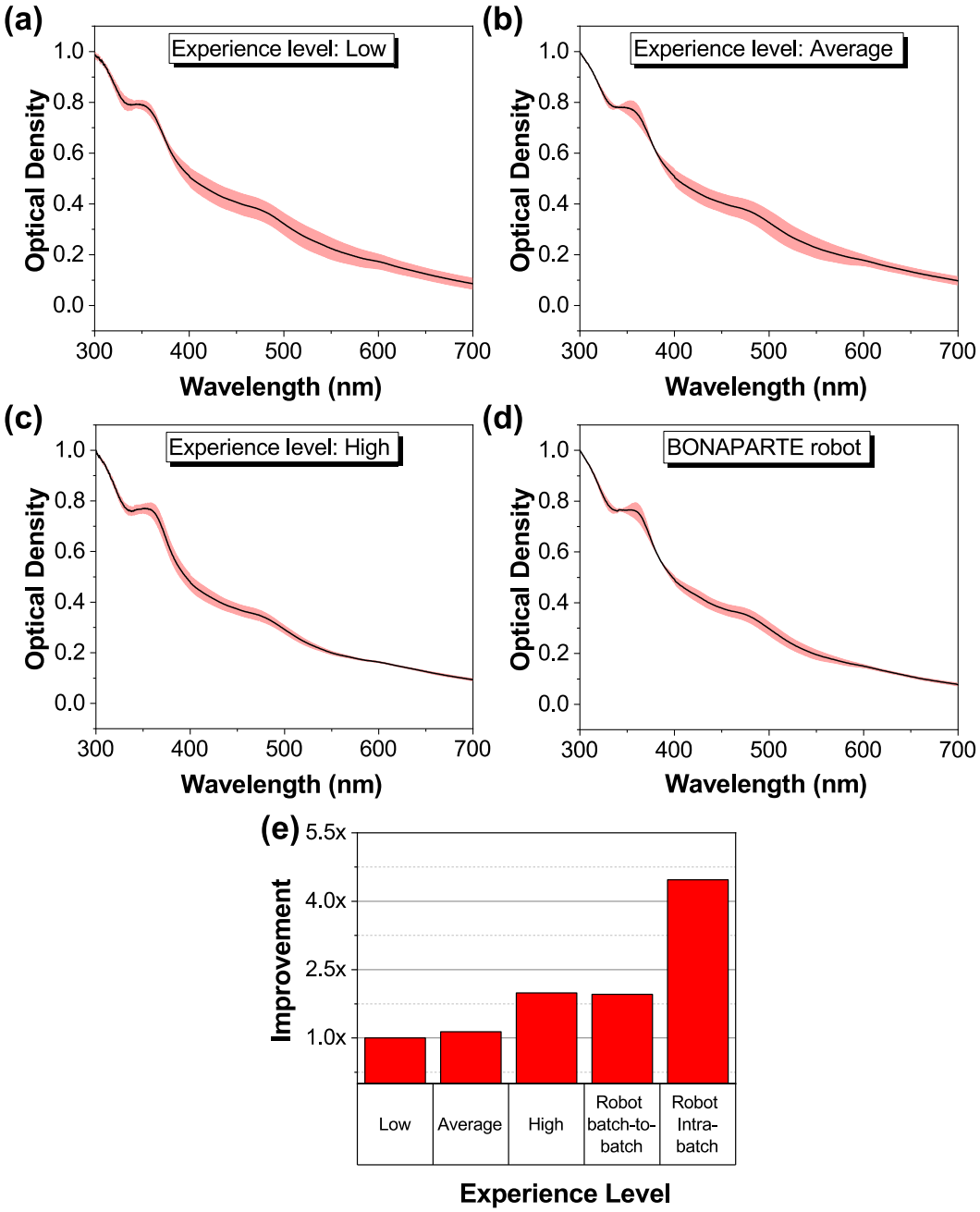


Figure 3 UV-Vis extinction spectra of syntheses performed manually (a-c, 14x, 15x and 6x repetitions, respectively) and by the BONAPARTE robot (d). Based on the standard deviation of the acquired spectra, an improvement factor was calculated (e), where the performance of the persons with the lowest experience is taken as a baseline.

**Pipetting speed in the synthesis of gold clusters**

Since the reaction is occurring on the scale of 1 s or even less and due to the fact the gold is reduced rapidly by $NaBH_4$, we hypothesized that the $NaBH_4$ solution has to be inserted rapidly into the solution.

In the above experiments we approximated the pipetting speed to be approximately 4 mL/s, and an offset pipetting position of 5 mm. To quantify the effects of both of these parameters we investigated them more closely. To quantify how fast pipetting is actually done, we measured the pipetting of 5 researchers from our group. The ejection speed was measured via slow-motion footage. The pipetting speed was determined to be 1.9 +- 0.4 mL/s. To determine if the pipetting speed has an influence on the particle size and distribution, we chose an ejection speed between 0.4 mL/s and 40 mL/s (maximum ejection speed of the robot). The pipetting speed of the robot was configured at four different values: 0.4, 0.8, 4, and 40 mL/s. The first and last values are used to probe the extremes and the others cover the range of pipetting speeds, that can be reasonably done by hand. Four of the syntheses were further analyzed by HRTEM. Due to the rapid addition of the educt it can be assumed that it mixed quicker and more uniformly, thus facilitating the rapid reduction of Au(I) to Au(0). The decrease in size and PdI observed at a flow rate of 40 mL/s as shown in Figure 4a and c, suggests this possibility. Representative TEM images can be found in Figure 4b1-b4 for the respective pipetting speeds. On the other hand, slow addition of $NaBH_4$ can lead to simultaneous growth and nucleation, which results in broader distributions with larger particles present. In turn, the average diameter increases. It should also be mentioned that despite the low pipetting speed, small gold clusters were synthesized even when injecting the whole volume on a time interval comparable to that in which the reaction itself usually happens. This could be explained by the stabilizing effect of the CTAB micelles on clusters, serving as a template and, thus, providing an upper limit to which the particles can grow.

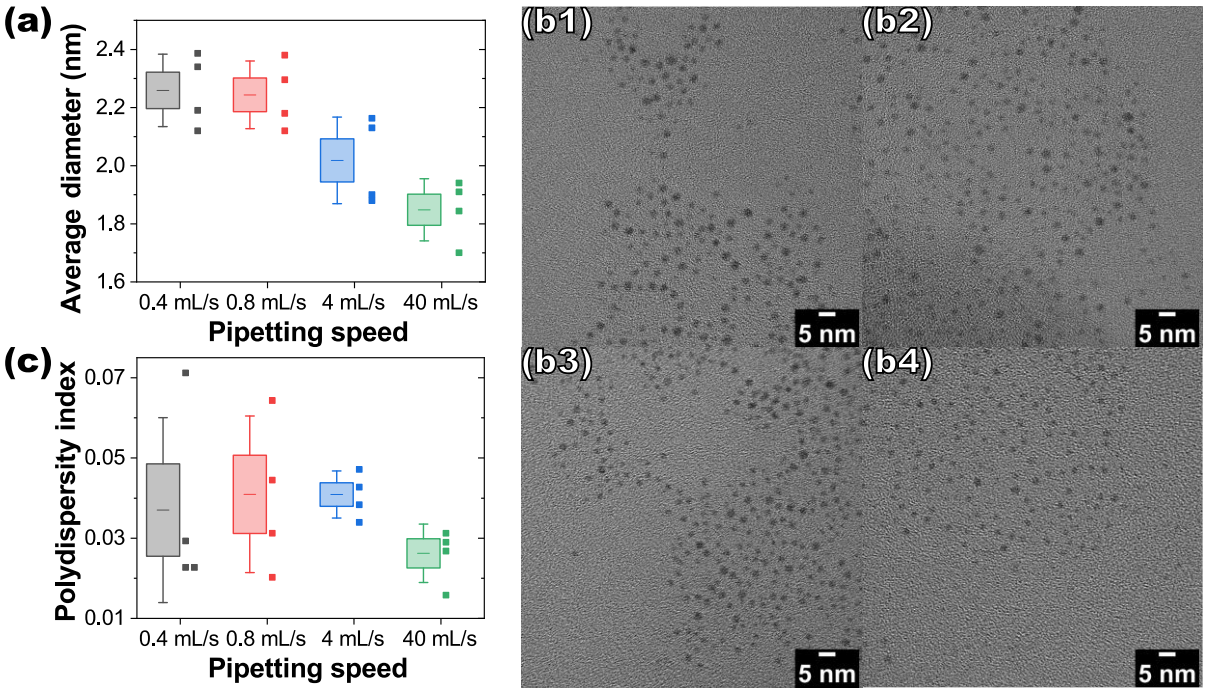


Figure 4: a) average particle diameter showing a tendency of decreasing with increasing pipetting speed as determined by HRTEM measurements of 4 syntheses. b) 1-4 HRTEM images of particles synthesized with 1: 0.4 mL/s, 2: 0.8 mL/s, 3: 4 mL/s, 4: 40 mL/s. c) – Polydispersity index of the particle populations as measured by HRTEM. A slight reduction is observed at 40 mL/s, possibly due to more rapid mixing between the educts. The error bars in a and c represent 1 standard deviation, while the box body 0.5 standard deviations.

These results agree with the Burst nucleation mechanism proposed by LaMer et al. [30] While no significant difference between syntheses is observed up to 4 mL/s, an improvement in PdI and a decrease in the size of the clusters is observed at 40 mL/s, a pipetting speed which is accessible by the robot, but not possible in manual pipetting. To summarize: 1) the robot can decrease the average cluster size by approximately 20% by increasing the pipetting speed to 40 mL/s, which is not accessible to common manual pipettes and 2) the robot can improve the PdI by approximately 30% at the speed of 40 mL/s.

**Pipetting position in the synthesis of gold clusters**

Additional to the pipetting speed we identified the pipetting position as a candidate for a critical parameter. This has been reported by experienced members of our group, the synthesis was more reproducible when pipetting the $NaBH_4$ off-center, meaning on the side of the formed vortex. To test this observation, we adjusted the offset parameter in the software and performed the synthesis with offsets of 0 mm (center of the vortex), 5 mm, 10 mm, and 15 mm. Figure 5a shows the average particle diameter, which was determined by TEM images (see Figure 5b1-4). Additionally, the polydispersity index is shown in Figure 5c. The total diameter of the glass vessel in which the synthesis was performed was approximately 19 mm. A minimum in particle size is reached with an offset of 10 mm, while smaller and larger offsets produce larger particle sizes. The vortex formed at 1500 RPM extends down to the stirring bar, meaning that when pipetting in the center of the vortex, the $NaBH_4$ solution comes first in contact with the stirring bar. At offsets of 5 mm and above, the $NaBH_4$ solution is directly pipetted into the stirred fluid. This could possibly affect the mixing efficiency. The mixing process has been investigated extensively in the field of anaerobic wastewater treatment reactors in order to increase the efficiency of the mass distribution and reactions. The approach, in that case, was to offset the stirring rod, which achieved more turbulent stirring conditions. In one study the efficiency of a reaction was increased by 10% by simply using an off-center stirring rod. [31] In our case, we offset the insertion of the educt, which could lead to enhanced mixing efficiency and thus faster distribution of the educt in the solution. These results are in good agreement with CFD simulations performed by Vite-Martínez et al. [32]

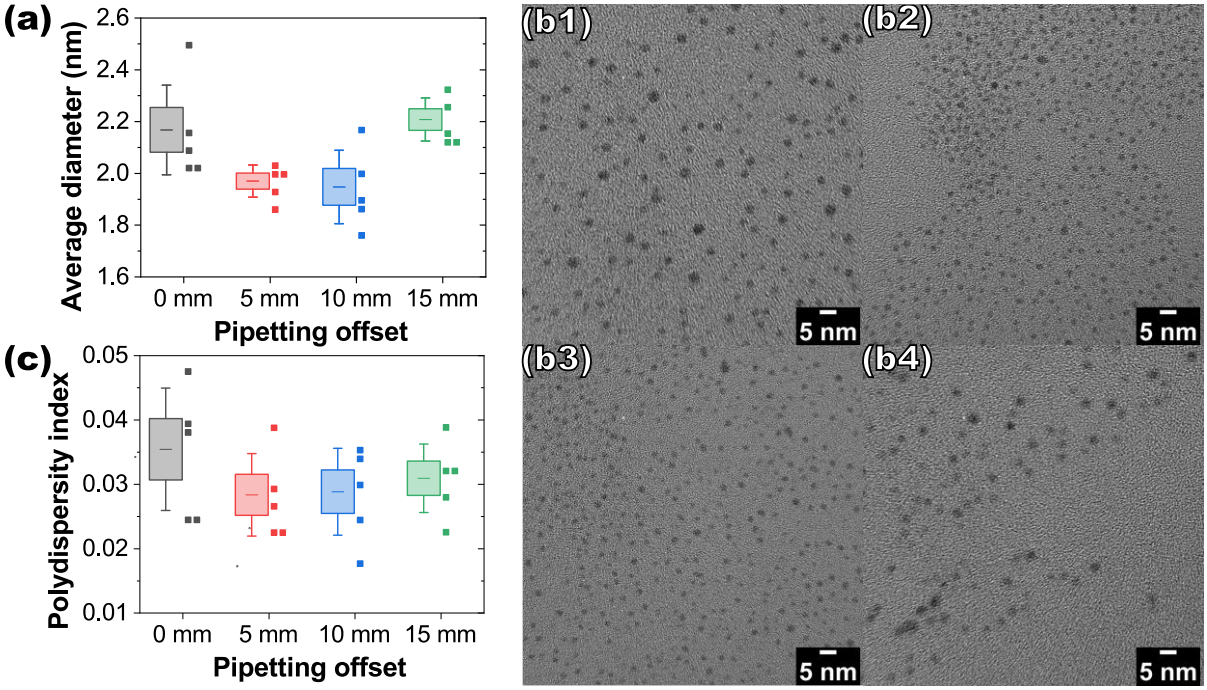


Figure 5: a) average particle diameter as determined by HRTEM shows a tendency of decreasing with increasing offset up to 10 mm with a sharp increase thereafter. b) 1-4 HRTEM images of particles synthesized with 1: 0 mm, 2: 5 mm, 3: 10 mm and 4: 15 mm offsets. c) – Polydispersity index of the particle populations as measured by TEM. No clear improvement can be seen at any specific offset. The error bars in a and c represent 1 standard deviation, while the box body 0.5 standard deviations.

It has been shown that the reproducible pipetting of substances into specific position in the solution influences the particle diameter. Pipetting directly in the center is disadvantageous, since the mixing of the educts is not optimal. Additionally, it may lead to the formation of reddish residues on the stirring bar itself (Figure S5) indicating the formation of a fraction of larger spherical particles. The use of the robot can completely eliminate this and increase the reproducibility of the synthesis.

**Synthesis of gold nanorods**

The gold clusters are usually prepared for use in the seed-based synthesis of gold nanoparticles with different morphologies. For SERS experiments, the plasmonically inactive clusters are usually grown to anisotropic particles of different shapes. Arguably, one of the most investigated syntheses of anisotropic particles both in theory [33–35] and practice [15, 36, 37] is the synthesis of gold nanorods. Therefore, this synthesis would be ideal to compare manual and robotic performance. We used the gold clusters for preparation of gold nanorods with a LSPR peak of 630 nm. The reproducibility of the synthesis based on the position of the longitudinal plasmonic mode was investigated first. The peak wavelength in every synthesis performed both manually and robotically is shown in Figure 6a. It can be observed that the number of outliers in the synthesis decreases with increasing experience level from six in the "low" group to three in the "average" and only one in the "high" experience group. Meanwhile no significant outliers were observed in the syntheses performed by BONAPARTE (Figure 6a purple). A further quantification of the improvement is shown in Figure 6b. Together with the average UV-Vis error (calculation described in the SI), both peak offset and peak scatter were calculated. The peak offset error is based on the average absolute deviation from the expected 630 nm LSPR peak wavelength. The robot achieved an improvement of 8-10x in all categories with significant improvements, even in comparison to a highly experienced person.

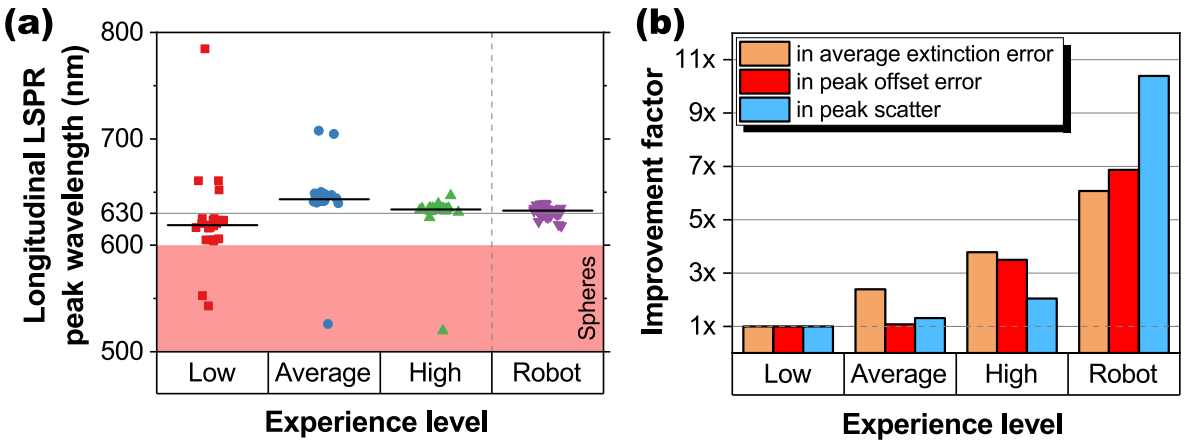


Figure 6 a) Longitudinal LSPR peak of the gold nanorods synthesized manually by persons of different experience levels and the BONAPARTE robot. An improvement is achieved in terms of peak offset and peak scatter. From 55 syntheses performed by BONAPARTE no significant outliers were observed. b) The improvement achieved by BONAPARTE in comparison to a low-experienced person outperforms that of both averagely and highly experienced persons performing the synthesis.

Due to the fact that the synthesis of nanorods does not include any time-critical steps, the improvement of the robot can be traced back to the improved pipetting performance. The added pipetting accuracy and precision seem to be the determining factors in the synthesis of gold nanorods.

The influence of the cluster population, however, cannot be excluded. In order to investigate the effect of the cluster size, we prepared 4 different batches of clusters with the following average cluster sizes (A: 1.93 nm; B: 2.22 nm; C: 2.57 nm; D: 2.71 nm). A series of gold nanorod syntheses were performed with each cluster population. The resulting gold nanorods were characterized by TEM (Figure 7c1-c4) in terms of length (Figure 7a) and width (Figure 7b). Note that the error bars do not represent the standard deviation of the length and width of the rods in one synthesis, but the standard deviation of the average length and average width between batches. The average width is little affected by the size distribution of the gold seeds (Figure S2). The overall width is probably determined by the symmetry-breaking event early into the growth of the nanorods, while there is a sufficient amount of gold atoms present in the solution. Therefore, it is possibly more influenced by the initial concentrations used, e.g. that of silver nitrate and CTAB, than the amount of clusters present. The average length seems to be dependent on the initial cluster population. With decreasing cluster size, the length of the rods decreases significantly. Possibly this is due to the smallest cluster population containing a higher particle number

density. Consequently, the amount of gold atoms from the growth solution per seed decreases. In general, the control of size and aspect ratio of the gold nanorods are important factors that determine their properties. For example, in biology, the uptake of nanoparticles is strongly size-dependent and for all applications where the LSPR peak wavelength is important the aspect ratio has to be precisely achieved. [38, 39]

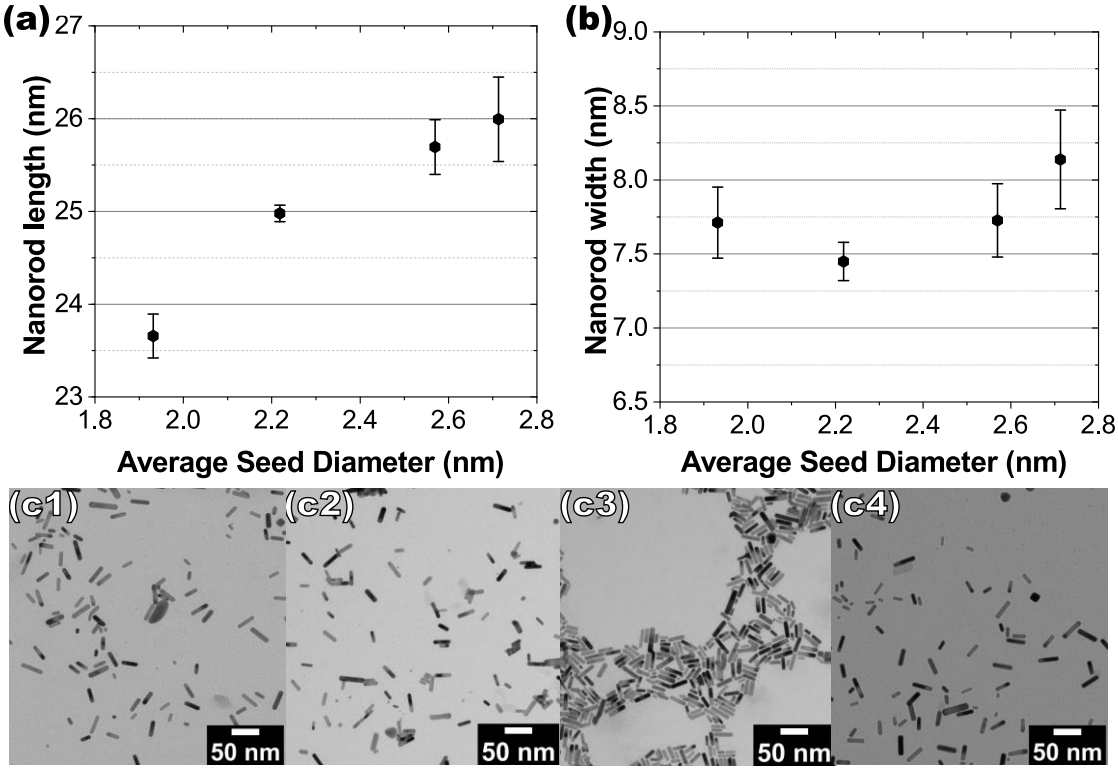


Figure 7 a) average length of nanorods synthesized with different cluster populations. A trend toward lower rod lengths when using smaller clusters can be observed. b) average width of nanorods synthesized with different cluster populations. The width remains relatively unaffected by the initial size of the Au clusters. The error bars represent the standard deviation of the batch-to-batch average length and width. c1-c4) representative TEM images of the rods synthesized with cluster populations A, B, C and D respectively.

In summary, the initial size of the clusters has a small but significant effect on the nanorod length. Using 1.93 nm instead of 2.71 nm clusters results in approximately 2.5 nm length decrease, corresponding to 10% of the total length. This shows that the average cluster size is important and effort has to be made not to control it reproducibly. The use of BONAPARTE for the synthesis of gold nanorods outperformed the manually performed synthesis both in achieving the desired LSPR peak wavelength and in reproducibility. Additionally, the experiments on the critical parameters, such as pipetting speed and pipetting position, show that the robot can control parameters, which would be impossible for a human to reproduce consistently.

**Synthesis of gold nanostars**

Previously, syntheses were performed where the critical step, usually the reduction step leading to the formation of the nanoparticles, was dependent only on one reactant. In order to exploit the fact that the robot has two automated pipettes available, we chose a synthesis where the critical step contains the addition of two educts in quick succession (approximately 1 s) and the time between the additions has a critical effect. This is the case in the protocol for the synthesis of nanostars first reported by Schütz et al. [40] The main advantage of this protocol is it avoids the use of toxic CTAB and DMF. Instead, it requires a growth solution containing $HAuCl_4$, $AgNO_3$ and trisodium citrate (growth solution), prepared seeds, and a hydroquinone solution. Following the protocol, for a successful synthesis the hydroquinone has to be added shortly after (1-2 seconds) the growth solution has been injected. The technical difficulty

lies in the rapid addition of the educts in quick succession. However, no exact quantification of the time delay between additions has been provided and it is left to interpretation. We decided to focus on 1 s delay. First, we compared the general performance of the robot versus manual syntheses. The results based on the LSPR peak wavelength from UV-Vis extinction measurements are shown in Figure 8a. Since more than one person participated in the "low" and "average" groups, the results are shown separately. In the "low" group the LSPR peaks of the resulting particles are blue-shifted compared to the expected wavelength (630 nm). Usually, this means that the time delay between the additions was shorter than required. One of the participants in the "average" group experienced particle aggregation, as can be seen by the redshift of the maxima to above 1000 nm. This is usually caused by insufficient cleaning of the labware. However, the second participant in the "average" group, the "high" group and the robot show results very close to the expected maximum. The improvement in the three different categories is shown in Figure 8b.

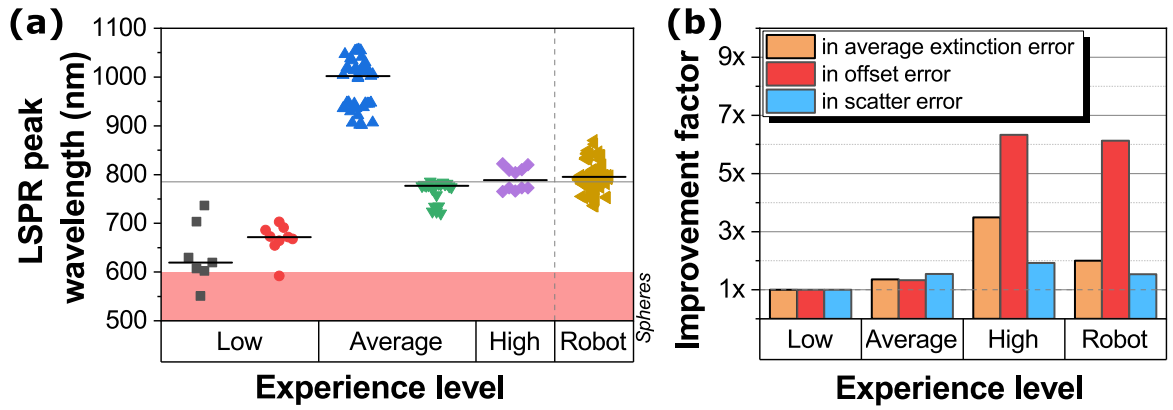


Figure 8 a) LSPR peak wavelength of the gold nanostars that were synthesized manually by persons of different experience levels and the BONAPARTE robot. A large deviation in the "low" and "average" groups underline the technically difficult nature of the synthesis. b) The improvement achieved by BONAPARTE in comparison to a low experienced person is similar to that of a highly experienced person and significantly outperforms both "low" and "averagely" experienced persons.

It is reasonable to assume that the time delay between additions is a crucial parameter in this synthesis protocol. Highly experienced individuals have a sense of the optimal delay, whereas the robot's delay is pre-programmed and consistent. Additionally, it can be observed that in the low group and part of the average group, there are systematic errors occurring. A blueshift of the peak usually indicates that the educts were pipetted simultaneously, while a significant redshift was previously observed to indicate either a too long delay or aggregation. The robot provides an improvement compared to these groups in terms of peak scatter which is an indicator of random errors (Figure 8b, blue). However, more significant is the improvement in peak offset, which is an indicator of systematic errors (Figure 8b, red). In order to investigate whether the systematic errors are caused by time delay deviations the synthesis was performed with different time delays: 1 s, 2 s, 5 s, 30 s (Figure 9a). The particle diameter as determined by TEM (Figure 9b1-b4) increases from about 115 nm to above 190 nm for all delays above 2 s. Particle histogram data can be found in the SI – Figure S4. In a previous work by Phiri et al. [41] it was found that nanostar formation is affected by the delayed addition of silver nitrate after the onset of reduction, in that case by ascorbic acid. In another study Yuan et al. came to the conclusion that the addition of silver and the reducing agent (ascorbic acid) has to be done simultaneously. Otherwise if added too early silver chloride precipitates from the solution and, if added too late, the particles have enough time to grow to larger spheres. [42] Since the reductant in both studies was ascorbic acid and not hydroquinone, the conclusions of these studies cannot be directly transferred to this case. However, the precipitation of AgCl cannot be excluded at longer time delays. It also has to be taken into account that the ionic strength of the seed solution increases significantly after the addition of the growth solution. This can lead to destabilization of the seeds and aggregation. Another factor is the possibility that the gold chloride has more time to form a shell-like structure around the particles, which, after the addition of the strong reducing agent, allows the particles to grow rapidly.

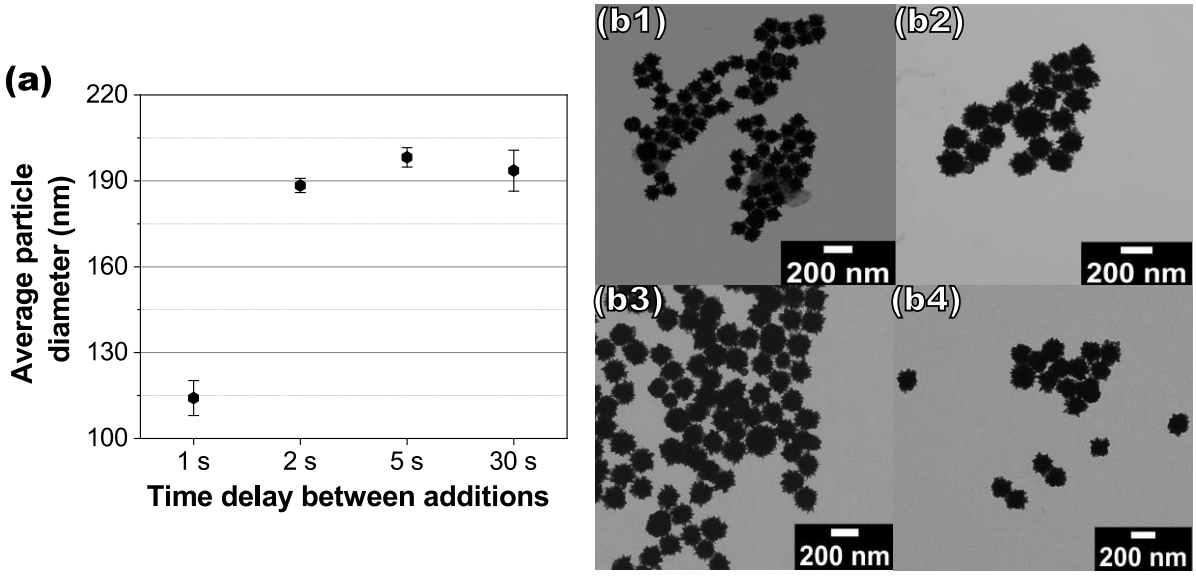


Figure 9 a) Average particle diameter as determined by TEM, after 2 s particles formed exhibit increased size. Each synthesis was repeated 3 times. The error bars represent the standard deviation of the batch-to-batch average diameter, not the standard deviation of the particle distribution. The actual particle distributions for each batch can be found in the supporting information. b1-b4) Corresponding TEM images (1 s, 2 s, 5 s, 30 s delay) of the particles.

The exact mechanism of the size increase after longer time delays is hard to deduce given this current dataset and requires further experiments. For example, the growth solution can be separated into gold chloride and citrate and be added before the silver and hydroquinone step. Another experiment may be performed by omitting hydroquinone completely to find out if and after what time small silver particles would form due to the reduction of the silver nitrate by citrate. Finally, the robot can be used to probe the interval between 1 s and 2 s, due to the size after 2 s remaining relatively unchanged.

## Conclusion

Our study introduces a nanoparticle synthesis robot that we developed using cost-effective 3D-printed parts. The performance of the robot is comparable, and in terms of pipetting accuracy and precision even surpasses commercially available options. Its customized design enabled us to investigate process parameters that had not been previously explored or quantified. The robot was used to examine little-explored synthesis parameters such as pipetting speed and pipetting position. It was found that they influence the size of the resulting particles. A 20% decrease in size was obtained by increasing the pipetting speed from 0.8 mL/s to 40 mL/s. The fact that the highest pipetting speeds are not accessible by manual pipetting, showcases the advantage of the robot. Another advantage of the rapid pipetting is that it facilitated a lower polydispersity index in the cluster syntheses. A similar decrease was seen by pipetting the educt with an offset from the middle of the synthesis vessel. Reproducing a specific offset by hand would be very difficult to achieve. Furthermore, we showed that using a smaller cluster population as seeds leads to an approximately 10% decrease in the length of nanorods. A significant improvement in the reproducibility of the synthesis of gold nanorods was observed in comparison to manual synthesis performed by persons of low, average and high experience levels.

In a separate study, the time delay between the addition of the growth solution and the reducing agent in the water-based hydroquinone synthesis of nanostars significantly influenced the final nanostar size. An increase in reproducibility was also observed, however, only compared to low and averagely experienced persons, but was slightly worse than that of highly experienced ones. This was caused by the technical difficulty of pipetting with 2 robotic pipettes in the same vessel, due to their large footprint. However, this can be solved by further miniaturization of the pipette system. Altogether, we showed that researchers have to take these synthesis process parameters such as pipetting speed, position and time delays into account and aim to better quantify and control them, which can be achieved with the help of customizable and automated synthesis platforms.

## Experimental section

### Chemicals

Gold(III)-chloride trihydrate ($HAuCl_4$ x 3 H2O, 99.9 %, Sigma-Aldrich), hexadecyltrimethylammoniumbromide (CTAB, 99 %, Sigma-Aldrich), Hydroquinone (Sigma Aldrich), hydrochloric acid (HCl, 1 M, Sigma-Aldrich), L-ascorbic acid (99 %, Sigma-Aldrich), silver nitrate ($AgNO_3$, 99.9999 %, Sigma-Aldrich), sodium borohydride $NaBH_4$, 98 %, Sigma-Aldrich), sodium citrate (99 %, Sigma-Aldrich). All chemicals were used as obtained.

### Preparation of stock solutions

For the gold clusters and rods, a CTAB 50 mM/Decanol 13.5 mM solution was used. A 10 mM Gold(III)-chloride solution is prepared and stored in a refrigerator. HCl was used as is. All other solutions were prepared fresh manually before a synthesis.

### Automated synthesis

Instructions for each synthesis are prepared beforehand by using our in-house software, developed in Python. Briefly, a synthesis is constructed by adding "synthesis steps" each with defined chemical (concentrations, volumes) and physical parameters (stirring, custom stirring profiles, pipetting speed, pipetting offset). These instructions are then parsed into a csv file, which can be loaded into the software and executed. An excel file with all XYZ positions of the synthesis modules, educt, spare pipetting units, and waste modules is also loaded by the software. For both the synthesis of small gold clusters and gold nanorods protocols were selected, which are commonly used in our lab, such as a modified version of the protocol proposed by Gonzales-Rubio et al. [36] Before each synthesis, glass vessels were cleaned first by ethanol and acetone to remove any organic residues from a previous synthesis, then rinsed with MilliQ ultrapure water. After that follows at least 10 minutes of stirring with aqua regia. Following, the vessel is rinsed with ethanol, acetone and MilliQ ultrapure water and left to dry at 100°C.

For the synthesis of the gold clusters, first, 10 mL CTAB/decanol solution is pipetted, which is followed by the addition of 500 µL HAuCl4 after which the solution turns yellow and then orange indicating the formation of CTAB-Au complexes. Then 50 µL ascorbic acid is added and the solution turns colorless after a couple of seconds. The last step is the addition of 400 µL of freshly prepared ice-cold $NaBH_4$ (20 mM). For the $NaBH_4$ refrigerated MilliQ-ultrapure water is used and the solution is further kept cool by a Peltier element integrated into the robot. All steps are performed at 500 RPM, except for the $NaBH_4$ pipetting, for which the stirring speed is increased by the robot to 1500 RPM, shortly before pipetting. For the pipetting speed experiments the robot 's pipetting speed was set to 0.4 mL/s; 0.8 mL/s; 4 mL/s and 40 mL/s respectively. For pipetting position experiments, an offset of 0 mm; 5 mm; 10 mm and 15 mm from the center of the vessel to the pipetting head was programmed. After 10 s the stirring is stopped altogether. UV-Vis extinction spectra are taken after 1 h of incubation with a JASCO V-730 spectrophotometer. For TEM characterization 1 mL of the seed solution is mixed with a dodecanethiol/THF solution. The particles separate from the solution and deposit as a thin layer on top of the solution, after which they are transfered with a pipette carefully to a 2 mL centrifuge tube containing 0.5 mL toluene. After some time CTAB leftover settles to the bottom of the solution and a TEM grid can be prepared avoiding most of the organic contamination. TEM grids are additionally plasma cleaned (Binder Labortechnik TPS 316) before measurement with a JEOL JEM-2200FS high-resolution TEM at 200 kV.

The seeded growth synthesis of gold nanorods is performed after 1 h incubation time of the clusters. Again 10 mL of the CTAB/decanol is pipetted into a 50 mL beaker, followed by 500 µL $HAuCl_4$ (10 mM), 40 µL 10 mM silver nitrate, 130 µL 100 mM ascorbic acid and 700 µL 1.0 M hydrochloric acid.

The final step consists of the pipetting of 850 µL seed particles. The solution is left for 5 minutes to stir and incubated overnight.

For the synthesis of nanostars 9.8 mL MilliQ-water with 300 uL of 40 nm seeds solution (OD 1) are prepared. Separately a solution consisting of 200 µL $HAuCl_4$ (1 wt% in water), 84 µL $AgNO_3$ (0,1 wt% in water), 26.6 µL trisodium citrate (1 wt% in water) is prepared and incubated for 5 min. This is referred to as growth solution. Another stock solution of hydroquinone (1 wt% in water) is prepared as well. The synthesis is initiated by setting the RPM to 650 and by holding a pipette in each hand (for short time delays, manual synthesis) the growth solution is pipetted. After the fixed time delay (1 s, 2 s, 5 s, 30 s), 100 µL hydroquinone in injected. The robot executes this step with its dual pipetting system. The solution turns to a dark blue-green color within seconds and is left to stir for 60 min. Following, the particles are centrifuged at 600 g for 30 min and redispersed in 1% PVP solution for stabilization.

| Step | | Gold clusters | Gold clusters (pipetting speed and position experiments) | Gold nanorods ($\lambda_{max}$ = 630 nm) | Gold nanorods ($\lambda_{max}$ = 785 nm) | Gold nanostars |
|---|---|---|---|---|---|---|
| 1 | Chemical | CTAB/Decanol (50 mM/13,5 mM) | CTAB/Decanol (50 mM/13,5 mM) | CTAB/Decanol (50 mM/13,5 mM) | CTAB/Decanol (50 mM/13,5 mM) | Deionized water |
| | Amount | 10 mL | 10 mL | 10 mL | 10 mL | 9,8 mL |
| | Process parameters | 400 RPM, 30°C | 400 RPM, 30°C | 400 RPM, 30°C | 400 RPM, 30°C | - |
| 2 | Chemical | $HAuCl_4$ (10 mM) | $HAuCl_4$ (10 mM) | $HAuCl_4$ (50 mM) | HAuCl4 (10 mM) | 40 nm seeds (OD 1) |
| | Amount | 500 µL | 500 µL | 100 µL | 500 µL | 300 µL |
| | Process parameters | 400 RPM, 30°C | 400 RPM, 30°C | 400 RPM, 30°C | 400 RPM, 30°C | - |
| 3 | Chemical | *L* -Ascorbic acid (100 mM) | *L* -Ascorbic acid (100 mM) | $AgNO_3$ (10 mM) | $AgNO_3$ (10 mM) | Growth solution (200 µL $HAuCl_4$ 1wt%; 84 µL $AgNO_3$ 0,1wt%; 26,6 µL $Na_3Cit$ 1wt%) |
| | Amount | 50 µL | 50 µL | 40 µL | 130 µL | Incubated for 5 minutes |
| | Process parameters | 400 RPM, 30°C | 400 RPM, 30°C | 400 RPM, 30°C | 400 RPM, 30°C | 650 RPM |
| 4 | Chemical | $NaBH_4$ (20 mM) | $NaBH_4$ (20 mM) | HCl (1M) | HCl (1M) | Hydroquinone |
| | Amount | 50 µL | 50 µL | 700 µL | 700 µL | 100 uL |
| | Process parameters | 1000 RPM, 30°C | Pipetting offsets: 0; 5; 10; 15 mm; 1500 RPM, 30°C at 40 mL/s<br>Pipetting speeds: 0,4; 0,8; 4; 40 mL/s; 1500 RPM, 30°C at 5 mm offset | 400 RPM, 30°C | 400 RPM, 30°C | 650 RPM, 1 s delay (2 s; 5 s; 30 s in time delay experiments) |
| 5 | Chemical | | | *L* -Ascorbic acid (100 mM) | *L* -Ascorbic acid (100 mM) | |
| | Amount | | | 130 µL | 130 µL | |
| | Process parameters | | | 400 RPM, 30°C | 400 RPM, 30°C | |
| 6 | Chemical | | | Clusters (OD 1,3 at 360 nm) | Clusters (as synthesized) | |
| | Amount | | | 750 µL | 850 µL | |
| | Process parameters | | | 400 RPM, 30°C | 400 RPM, 30°C | |

**References**


[1] K. Sztandera, M. Gorzkiewicz, and B. Klajnert-Maculewicz, "Gold Nanoparticles in Cancer Treatment," *Molecular Pharmaceutics*, early access. doi: 10.1021/acs.molpharmaceut.8b00810.

[2] M. S. Kang, S. Y. Lee, K. S. Kim, and D.-W. Han, "State of the Art Biocompatible Gold Nanoparticles for Cancer Theragnosis," *Pharmaceutics*, early access. doi: 10.3390/pharmaceutics12080701.

[3] V. Amendola, R. Pilot, M. Frasconi, O. M. Maragò, and M. A. Iatì, "Surface plasmon resonance in gold nanoparticles: a review," *Journal of physics. Condensed matter : an Institute of Physics journal*, vol. 29, no. 20, p. 203002, 2017, doi: 10.1088/1361-648X/aa60f3.

[4] M. Falahati *et al.,* "Gold nanomaterials as key suppliers in biological and chemical sensing, catalysis, and medicine," *Biochimica et biophysica acta. General subjects*, early access. doi: 10.1016/j.bbagen.2019.129435.

[5] Á. I. López-Lorente, "Recent developments on gold nanostructures for surface enhanced Raman spectroscopy: Particle shape, substrates and analytical applications. A review," *Analytica Chimica Acta*, early access. doi: 10.1016/j.aca.2021.338474.

[6] C. Burda, X. Chen, R. Narayanan, and M. A. El-Sayed, "Chemistry and properties of nanocrystals of different shapes," *Chemical reviews*, vol. 105, no. 4, pp. 1025–1102, 2005, doi: 10.1021/cr030063a.

[7] J. Reguera, J. Langer, D. Jiménez de Aberasturi, and L. M. Liz-Marzán, "Anisotropic metal nanoparticles for surface enhanced Raman scattering," *Chemical Society reviews*, vol. 46, no. 13, pp. 3866–3885, 2017, doi: 10.1039/c7cs00158d.

[8] M. R. K. Ali, Y. Wu, and M. A. El-Sayed, "Gold-Nanoparticle-Assisted Plasmonic Photothermal Therapy Advances Toward Clinical Application," *J. Phys. Chem. C*, vol. 123, no. 25, pp. 15375–15393, 2019, doi: 10.1021/acs.jpcc.9b01961.

[9] Y. Wu, M. R. Ali, K. Chen, N. Fang, and M. A. El-Sayed, "Gold nanoparticles in biological optical imaging," *Nano Today*, vol. 24, pp. 120–140, 2019, doi: 10.1016/j.nantod.2018.12.006.

[10] A. K. Pearce, T. R. Wilks, M. C. Arno, and R. K. O'Reilly, "Synthesis and applications of anisotropic nanoparticles with precisely defined dimensions," *Nature reviews. Chemistry*, early access. doi: 10.1038/s41570-020-00232-7.

[11] I. García, M. Henriksen-Lacey, J. Calvo, D. J. de Aberasturi, M. M. Paz, and L. M. Liz-Marzán, "Size-Dependent Transport and Cytotoxicity of Mitomycin-Gold Nanoparticle Conjugates in 2D and 3D Mammalian Cell Models," *Bioconjugate chemistry*, early access. doi: 10.1021/acs.bioconjchem.8b00898.

[12] J. Mosquera, I. García, and L. M. Liz-Marzán, "Cellular Uptake of Nanoparticles versus Small Molecules: A Matter of Size," *Accounts of chemical research*, early access. doi: 10.1021/acs.accounts.8b00292.

[13] J. W. Trzciński, L. Panariello, M. O. Besenhard, Y. Yang, A. Gavriilidis, and S. Guldin, "Synthetic guidelines for the precision engineering of gold nanoparticles," *Current Opinion in Chemical Engineering*, vol. 29, pp. 59–66, 2020, doi: 10.1016/j.coche.2020.05.004.

[14] L. M. Liz-Marzán, C. R. Kagan, and J. E. Millstone, "Reproducibility in Nanocrystal Synthesis? Watch Out for Impurities!," *ACS nano*, vol. 14, no. 6, pp. 6359–6361, 2020, doi: 10.1021/acsnano.0c04709.

[15] G. González-Rubio *et al.,* "Disconnecting Symmetry Breaking from Seeded Growth for the Reproducible Synthesis of High Quality Gold Nanorods," *ACS nano*, early access. doi: 10.1021/acsnano.8b09658.

[16] M. Christensen *et al.,* "Automation isn't automatic," *Chemical science*, early access. doi: 10.1039/d1sc04588a.

[17] J. Bai, L. Cao, S. Mosbach, J. Akroyd, A. A. Lapkin, and M. Kraft, "From Platform to Knowledge Graph: Evolution of Laboratory Automation," *JACS Au*, early access. doi: 10.1021/jacsau.1c00438.

[18] B. Pinho and L. Torrente-Murciano, "Dial-A-Particle: Precise Manufacturing of Plasmonic Nanoparticles Based on Early Growth Information—Redefining Automation for Slow Material Synthesis," *Adv. Energy Mater.*, vol. 11, no. 32, p. 2100918, 2021, doi: 10.1002/aenm.202100918.

[19] H. Huang, H. Du Toit, L. Panariello, L. Mazzei, and A. Gavriilidis, "4. Continuous synthesis of gold nanoparticles in micro- and millifluidic systems," in *Metallic Nanomaterials: Chemistry in Practice* (De Gruyter Textbook Ser), L. García-Cruz et al., Eds., Berlin/Boston: De Gruyter, Inc, 2018, pp. 157–220.

[20] A. M. Salaheldin *et al.,* "Automated synthesis of quantum dot nanocrystals by hot injection: Mixing induced self-focusing," *Chemical Engineering Journal*, vol. 320, pp. 232–243, 2017, doi: 10.1016/j.cej.2017.02.154.

[21] E. M. Chan *et al.,* "Reproducible, high-throughput synthesis of colloidal nanocrystals for optimization in multidimensional parameter space," *Nano letters*, vol. 10, no. 5, pp. 1874–1885, 2010, doi: 10.1021/nl100669s.

[22] Y. Fan *et al.,* "Automated high-throughput preparation and characterization of oligonucleotide-loaded lipid nanoparticles," *International journal of pharmaceutics*, early access. doi: 10.1016/j.ijpharm.2021.120392.

[23] Y. Jiang, D. Salley, A. Sharma, G. Keenan, M. Mullin, and L. Cronin, "An artificial intelligence enabled chemical synthesis robot for exploration and optimization of nanomaterials," *Science advances*, early access. doi: 10.1126/sciadv.abo2626.

[24] H. Zhao *et al.,* "A robotic platform for the synthesis of colloidal nanocrystals," *Nat. Synth*, 2023, doi: 10.1038/s44160-023-00250-5.

[25] G. Muralidharan, L. Subramanian, S. K. Nallamuthu, V. Santhanam, and S. Kumar, "Effect of Reagent Addition Rate and Temperature on Synthesis of Gold Nanoparticles in Microemulsion Route," *Ind. Eng. Chem. Res.*, vol. 50, no. 14, pp. 8786–8791, 2011, doi: 10.1021/ie2002507.

[26] M. Baker, "1,500 scientists lift the lid on reproducibility," *Nature*, vol. 533, no. 7604, pp. 452–454, 2016, doi: 10.1038/533452a.

[27] N. R. Jana, L. Gearheart, and C. J. Murphy, "Evidence for Seed-Mediated Nucleation in the Chemical Reduction of Gold Salts to Gold Nanoparticles," *Chem. Mater.*, vol. 13, no. 7, pp. 2313–2322, 2001, doi: 10.1021/cm000662n.

[28] K. Huang *et al.,* "One-step synthesis of 3D dendritic gold/polypyrrole nanocomposites via a self-assembly method," *Nanotechnology*, vol. 17, no. 1, pp. 283–288, 2006, doi: 10.1088/0957-4484/17/1/048.

[29] M. O. Besenhard, R. Baber, A. P. LaGrow, L. Mazzei, N. T. K. Thanh, and A. Gavriilidis, "New insight into the effect of mass transfer on the synthesis of silver and gold nanoparticles," *CrystEngComm*, vol. 20, no. 44, pp. 7082–7093, 2018, doi: 10.1039/C8CE01014E.

[30] V. K. LaMer and R. H. Dinegar, "Theory, Production and Mechanism of Formation of Monodispersed Hydrosols," *J. Am. Chem. Soc.*, vol. 72, no. 11, pp. 4847–4854, 1950, doi: 10.1021/ja01167a001.

[31] Y. Huang, F. MahmoodPoor Dehkordy, Y. Li, S. Emadi, A. Bagtzoglou, and B. Li, "Enhancing anaerobic fermentation performance through eccentrically stirred mixing: Experimental and modeling methodology," *Chemical Engineering Journal*, vol. 334, pp. 1383–1391, 2018, doi: 10.1016/j.cej.2017.11.088.

[32] P. Vite-Martínez, C. Durán-Valencia, J. A. Cruz-Maya, A. Ramírez-López, and S. López-Ramírez, "Optimization of reagents injection in a stirred batch reactor by numerical simulation," *Computers & Chemical Engineering*, vol. 60, pp. 307–314, 2014. doi: 10.1016/j.compchemeng.2013.09.005. [Online]. Available: https://www.sciencedirect.com/science/article/pii/s0098135413002743

[33] J. A. Da Silva, P. A. Netz, and M. R. Meneghetti, "Growth Mechanism of Gold Nanorods: the Effect of Tip-Surface Curvature As Revealed by Molecular Dynamics Simulations," *Langmuir : the ACS journal of surfaces and colloids*, early access. doi: 10.1021/acs.langmuir.9b03235.

[34] J. A. Da Silva and M. R. Meneghetti, “New Aspects of the Gold Nanorod Formation Mechanism via Seed-Mediated Methods Revealed by Molecular Dynamics Simulations,” *Langmuir : the ACS journal of surfaces and colloids*, early access. doi: 10.1021/acs.langmuir.7b03703.

[35] S. K. Meena and M. Sulpizi, “From Gold Nanoseeds to Nanorods: The Microscopic Origin of the Anisotropic Growth,” *Angewandte Chemie (International ed. in English)*, early access. doi: 10.1002/anie.201604594.

[36] G. González-Rubio, L. Scarabelli, A. Guerrero-Martínez, and L. M. Liz-Marzán, “Surfactant-Assisted Symmetry Breaking in Colloidal Gold Nanocrystal Growth,” *ChemNanoMat*, vol. 6, no. 5, pp. 698–707, 2020, doi: 10.1002/cnma.201900754.

[37] E. Carbó-Argibay *et al.,* “The crystalline structure of gold nanorods revisited: evidence for higher-index lateral facets,” *Angewandte Chemie (International ed. in English)*, vol. 49, no. 49, pp. 9397–9400, 2010, doi: 10.1002/anie.201004910.

[38] J. Song *et al.,* “Ultrasmall Gold Nanorod Vesicles with Enhanced Tumor Accumulation and Fast Excretion from the Body for Cancer Therapy,” *Advanced materials (Deerfield Beach, Fla.)*, early access. doi: 10.1002/adma.201502486.

[39] F. Zhao *et al.,* “Activatable ultrasmall gold nanorods for "off-on" fluorescence imaging-guided photothermal therapy,” *Journal of materials chemistry. B*, early access. doi: 10.1039/c6tb02873j.

[40] M. Schütz, D. Steinigeweg, M. Salehi, K. Kömpe, and S. Schlücker, “Hydrophilically stabilized gold nanostars as SERS labels for tissue imaging of the tumor suppressor p63 by immuno-SERS microscopy,” *Chemical communications (Cambridge, England)*, early access. doi: 10.1039/c0cc05229a.

[41] M. M. Phiri, D. W. Mulder, and B. C. Vorster, “Seedless gold nanostars with seed-like advantages for biosensing applications,” *Royal Society open science*, early access. doi: 10.1098/rsos.181971.

[42] H. Yuan, C. G. Khoury, H. Hwang, C. M. Wilson, G. A. Grant, and T. Vo-Dinh, “Gold nanostars: surfactant-free synthesis, 3D modelling, and two-photon photoluminescence imaging,” *Nanotechnology*, early access. doi: 10.1088/0957-4484/23/7/075102.

## Acknowledgements

We thank the Center for Nanointegration Duisburg-Essen (CENIDE) and the Interdisciplinary Center for Analytics on the Nanoscale (ICAN) for the technical support and especially Dr. Markus Heidelmann for the HRTEM nanoparticle characterizations.